Volume 2

Application of relations between seismic amplitude, velocity and lithology in geological interpretation of seismic data

Smiljan Prskalo[1]

1INA d.d Naftaplin, Zagreb, Croatia, E-mail: sprskalo@ina.hr

Abstract

Geological interpretation of seismic data should fulfill two main objectives: solving geometry of structures with possible hydrocarbon accumulations and correlation of recorded seismic amplitudes and velocities with lithology. The first objective is easily achieved through already well established procedures of structural interpretation, while the second one is still based on factors highly depending on interpreters' previous experiences. In order to establish some reliable criteria for interpretation lithology and fluid saturation of possible interesting reservoir rocks, relation between physical rock properties (density, elasticity, fluid saturation) and seismic waves velocity and amplitudes were already analyzed and presented in many so far publicized works. According to them seismic velocities depend on rock elasticity and density, i.e. on rock lithology. As the reflected seismic wave amplitudes are functions of acoustic impedances – product of velocity and density – therefore they can be interpreted in terms of rock properties (lithology, fluid type and saturation), and even used as direct hydrocarbon indicators.

In the article mathematical relations between elasticity, velocity and amplitude are presented according to the known, already publicized works listed in Reference. Short description of physical meaning of these formulae, as well as discussion of their practical applications, is done in the next part. Finally, some examples of hydrocarbon – particularly gas – reservoir exploration on Adriatic Sea are presented in order to illustrate real possibilities of this approach to seismic data interpretation.

Keywords: seismic, amplitude, velocity, geological interpretation, Adriatic Sea

INTRODUCTION

The main objective of seismic data application in hydrocarbon exploration has not been changed during the last 40 years. At the same time the technology of seismic methods has drastically improved and enabled exploration geophycists to meet many times higher demands involving seismic methods in every day use in reservoir exploration and development.

Oil and gas accumulations could be formed in structural and stratigraphic traps. The definition of underground geometry is based on the times needed for seismic wave to travel the path source – reflector – receiver. The procedure of structural interpretation is today well established, relatively not very demanding procedure, highly performed using powerful computers. In other words, following certain rules concerning seismic reflections picking on the properly processed 2D or 3D data presentations, and their correlation with well data, a reliable geological model of the explored underground could be established.
The first attempts of solving lithology and oil and gas finding by seismic methods are connected with the commencement of seismic methods practical applications. Due to the fact that these tasks can be solved by analyzing seismic wave characteristics (amplitude, frequency, polarity, velocity) using seismic data of excellent quality, such information became available only after successful advances in seismic technology. However, seismic amplitudes analysis in at least qualitative lithology determinations, were practically used all the time, in spite to the lack of publicized works, mainly due to keeping such procedures as big companies' secrets.
Theoretical background for seismic amplitude interpretation, necessary in recently developed AVO (Amplitude-Versus-Offset) method has been already established at the beginning of the last century. In the Knott's and Zoeppritz's works (Knott, 1899, Zoeppritz, 1919) the seismic amplitude dependence on seismic velocity and density in two layer medium were analyzed. Based on these works, equations describing amplitude changes as functions of P and S wave velocities, density and angle of incidence of seismic arrival on the reflector, were developed. These equations were rather very complex and therefore it was very difficult, practically almost impossible, to find their solutions.
During later years it was attempted to simplify them in order to make them usable in practice. Petrophysical link to seismic data was described by Gassmann (Gassmann, 1951) in his 1951 article. In this article, publicized in 1955, Koefoed (Koefoed, 1955) presented an expression describing offset dependent amplitude change and established theoretical background for in the future very popular AVO method. The first systematic attempt in lithology prognosis through reflection coefficients analysis was described by Rosa (Rosa, 1976). Further development in practical use of amplitudes in lithology and fluid saturation is connected with the works of Ostrander (Ostrander, 1982 and 1984). In the 1985 Shuey (Shuey, 1985) publicized the article on linear approximation equation later widely used in practical application of AVO method.

SEISMIC VELOCITIES VERSUS ROCK PHYSICS

Force impulse acting on the surface results in spreading volume P and S wave along rays starting in the seismic source. Seismic wave fronts in the homogeneous medium are symmetric spheres with curvatures continuously increasing as the distance from the source increases. At the very long distance (theoretically close to infinity) the wave fronts became planes, and rays linear. These approximations are used in the following derivations. Accordingly, seismic velocities change only at the reflecting surfaces between two media (layers), making easier further theoretical analysis.
Under the stress, the observed point moves from its original position $\mathbf{P}(x_0, y_0, z_0)$ to the new position $\mathbf{P}(x_0+\Delta x, y_0+\Delta y, z_0+\Delta z)$ in Cartesian coordinates, as shown on ***Fig.1.*** Resulting shifts in the 3 directions, shown on the figure are defined as $\Delta x = u$, $\Delta y = v$ and $\Delta z = w$.
The linear strains ε_{xx}, ε_{yy}, ε_{zz} in the ***x, y*** and ***z*** directions are equal to the changes in lengths per unit lengths defined by expressions

$$\varepsilon_{xx} = \frac{\partial u}{\partial x}, \quad \varepsilon_{yy} = \frac{\partial v}{\partial y}, \quad \varepsilon_{zz} = \frac{\partial w}{\partial z} \tag{1}$$

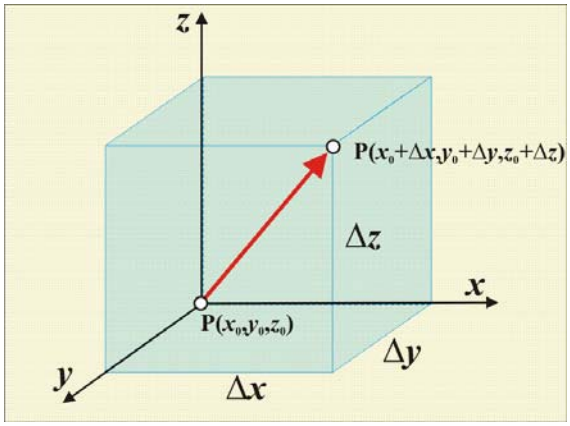

Fig.1: Point position change under stress

Volume strain, θ, or dilatation is the change in volume per unit volume, defined by

$$\theta = \frac{\partial u}{\partial x} + \frac{\partial v}{\partial y} + \frac{\partial w}{\partial z} = \varepsilon_{xx} + \varepsilon_{yy} + \varepsilon_{zz} \tag{2}$$

The ratio of lateral contraction to linear extension in a strained element is Poisson ratio. Such extension in the ***x***-direction is defined by following relations

$$\sigma = \frac{\partial v/\partial y}{\partial u/\partial x} = \frac{\varepsilon_{yy}}{\varepsilon_{xx}}$$
$$\sigma = \frac{\partial w/\partial z}{\partial u/\partial x} = \frac{\varepsilon_{zz}}{\varepsilon_{xx}} \tag{3}$$

Stress is defined as the ratio of force to area, in the limit, as the area approaches zero value. On ***Fig. 2*** components of stress acting in the ***x***, ***y*** and ***z*** directions are shown.

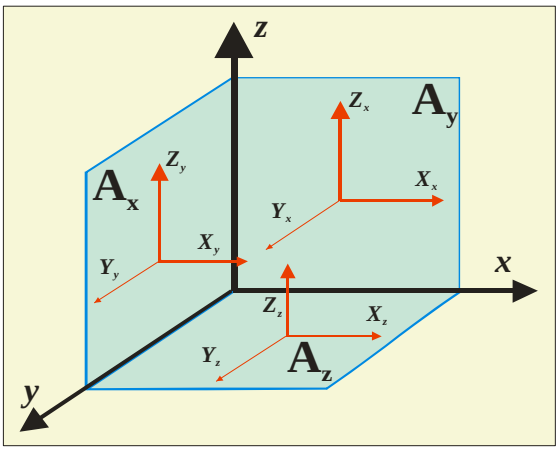

Fig.2: Stress components

The nine components of stress, X_x, X_y, X_z, Y_x, Y_y, Y_z, Z_x, Z_y, Z_z, are shown on the figure. The capital letter indicates the direction of stress and the subscript indicates the direction of the normal to the surface. To maintain equilibrium, the components of shear stress must satisfy relations:

$$X_y = Y_x, \quad X_z = Z_x, \quad Y_z = Z_y \tag{4}$$

With the 3 compress ional stress components X_x, Y_y and Z_z they form a total of six independent stress components. According to Hook's law the stress is proportional to the strain. In general, each of the six independent components of stress at a point (X_x, Y_y, Z_z, X_y, X_z, Y_z) is linear functions of the six independent components of strain (ε_{xx}, ε_{yy}, ε_{zz}, ε_{xy}, ε_{yz}, ε_{zx}). This results in 36 elastic constants, 21 of which are independent if no symmetry exists. In a homogeneous and isotropic material, the number of independent elastic constants is reduced to the Lame constants, λ and μ, and stress-strain relations become

$$\begin{aligned} &X_x = \lambda\theta + 2\mu\varepsilon_{xx}, \quad Y_y = \lambda\theta + 2\mu\varepsilon_{yy}, \quad Z_y = \lambda\theta + 2\mu\varepsilon_{zz}, \quad and \\ &X_y = Y_x = \mu\varepsilon_{xy} = \mu\varepsilon_{yx}, \quad X_z = Z_x = \mu\varepsilon_{xz} = \mu\varepsilon_{zx}, \quad Y_z = Z_y = \mu\varepsilon_{yz} = \mu\varepsilon_{zy} \end{aligned} \tag{5}$$

In the case of purely compressional stress applied in the x-direction when all other stress components are equal to zero, and after substituting θ with right hand side of equation (2), the first three equations in (5) became

$$\begin{aligned} X_x &= (\lambda + 2\mu)\cdot\varepsilon_{xx} + \lambda\cdot(\varepsilon_{yy} + \varepsilon_{zz}) \\ 0 &= (\lambda + 2\mu)\cdot\varepsilon_{yy} + \lambda\cdot(\varepsilon_{xx} + \varepsilon_{zz}) \\ 0 &= (\lambda + 2\mu)\cdot\varepsilon_{zz} + \lambda\cdot(\varepsilon_{xx} + \varepsilon_{yy}) \end{aligned} \tag{6}$$

Solving for ε_{xx}, ε_{yy}, ε_{zz} gives

$$\varepsilon_{xx} = \frac{\lambda + \mu}{\mu(3\lambda + 2\mu)}\cdot X_x \qquad and \qquad \varepsilon_{yy} = \varepsilon_{zz} = \frac{\lambda}{2\mu(3\lambda + 2\mu)}\cdot X_x \tag{7}$$

Young's modulus E, and Poisson's ratio σ, shown on ***Fig.3***, are defined as follows

$$\begin{aligned} E &= \frac{X_x}{\varepsilon_{xx}} = \frac{\mu(3\lambda + 2\mu)}{\lambda + \mu} = \frac{F/A}{\Delta L/L} \quad i \\ \sigma &= \frac{\varepsilon_{yy}}{\varepsilon_{xx}} = \frac{\lambda}{2(\lambda + \mu)} = \frac{\Delta D/D}{\Delta L/L} \end{aligned} \tag{8}$$

Under uniform hydrostatic pressure on the unit sphere normal stress components X_x, Y_y and Z_z are equal to the pressure P, while the shear stress components became 0. According to this, stress-strain relation is defined by

$$\varepsilon_{xx} = \varepsilon_{yy} = \varepsilon_{zz} = -\frac{P}{3\lambda + 2\mu} \tag{9}$$

Volume change $\theta = \Delta Vol/Vol$ defines bulk modulus k according to the relation

$$k = \frac{P}{\theta} = \frac{P}{\varepsilon_{xx} + \varepsilon_{yy} + \varepsilon_{zz}} = \lambda + \frac{2}{3}\mu = \frac{P}{\Delta Vol/Vol} \tag{10}$$

Seismic wave arrival on the side of unit cube with the angle different from 90^0, as shown in lower right angle of ***Fig. 3***, causes shear defined by elastic shear modulus μ depending on the stress F/A and the length of cube's side $\Delta D/D$, according to the following relation

$$\mu = \frac{\tau}{tg\,\phi} = \frac{F/A}{\Delta D/D} \tag{11}$$

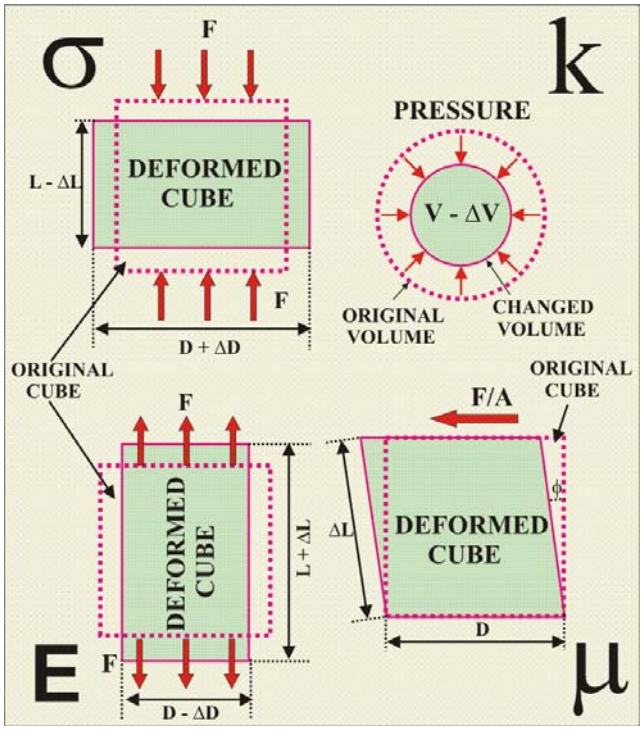

Fig.3: Elastic constants

After combining the above relations Lame's constant λ is derived as

$$\lambda = \frac{\sigma \cdot E}{(1+\sigma)\cdot(1-2\sigma)} \tag{12}$$

According to the relations shown on ***Fig.4***, the difference between components of X_x stress acting on opposite **ABCD** and **EFGH** sides, is defined as follows

$$\left(X_x + \frac{\partial X_x}{\partial x}\Delta x\right) - X_x = \frac{\partial X_x}{\partial x}\Delta x \tag{13}$$

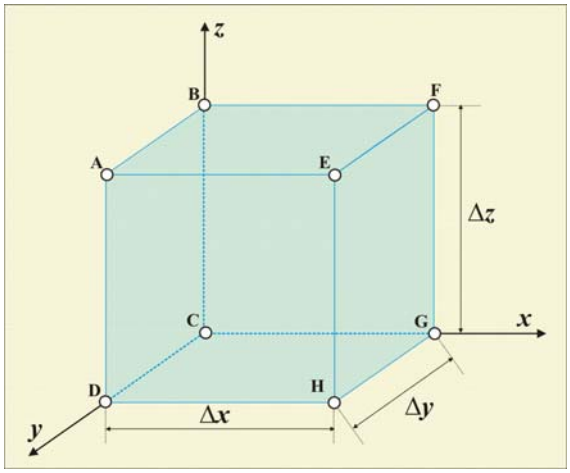

Fig.4: Stress acting on the unit cube

Resulting force F_x is equal to the stress X_x multiplied with the surface area $\Delta y \Delta z$ on which it is acting, i.e.:

$$F_x = \left(\frac{\partial X_x}{\partial x} \Delta x \right) \cdot (\Delta y \Delta z) \tag{14}$$

The forces, F_y and F_z, acting on the other two sides are

$$F_y = \left(\frac{\partial X_y}{\partial y} \Delta y \right) \cdot (\Delta x \Delta z), \qquad F_z = \left(\frac{\partial X_z}{\partial z} \Delta z \right) \cdot (\Delta x \Delta y) \tag{15}$$

According to the second Newton's law $F_x = ma_x$, after mass m is replaced by product of density ρ and change of volume $\rho \Delta x \Delta y \Delta z$, and acceleration a_x with the second partial derivation of shift u per time t, the following relation is obtained

$$F_x = ma_x \rightarrow \left(\frac{\partial X_x}{\partial x} + \frac{\partial X_y}{\partial y} + \frac{\partial X_z}{\partial z} \right) = \rho \frac{\partial^2 u}{\partial t^2} \tag{16}$$

The expressions for forces F_y and F_z, acting in the other two directions are similar. Obviously in them only need to replace the shift u on the right hand side of the equation with v or w.

In the homogeneous isotropic medium, after introducing elastic constants, the above equations became

$$\begin{aligned}
(\lambda + \mu) \frac{\partial \theta}{\partial x} + \mu \left(\frac{\partial^2 u}{\partial x^2} + \frac{\partial^2 u}{\partial y^2} + \frac{\partial^2 u}{\partial z^2} \right) &= \rho \frac{\partial^2 u}{\partial t^2} \\
(\lambda + \mu) \frac{\partial \theta}{\partial y} + \mu \left(\frac{\partial^2 v}{\partial x^2} + \frac{\partial^2 v}{\partial y^2} + \frac{\partial^2 v}{\partial z^2} \right) &= \rho \frac{\partial^2 v}{\partial t^2} \\
(\lambda + \mu) \frac{\partial \theta}{\partial z} + \mu \left(\frac{\partial^2 w}{\partial x^2} + \frac{\partial^2 w}{\partial y^2} + \frac{\partial^2 w}{\partial z^2} \right) &= \rho \frac{\partial^2 w}{\partial t^2}
\end{aligned} \tag{17}$$

For the plane wave spreading only in x-direction, all members with partial derivation in y and z directions are equal to 0, and the partial derivation of change θ per unit distance in x-direction is equal to the following relation

$$\frac{\partial \theta}{\partial x} = \frac{\partial^2 u}{\partial x^2} \tag{18}$$

The final equations describing plane wave spreading became as follows

$$\begin{aligned}
\frac{\partial^2 u}{\partial t^2} &= \frac{\lambda + 2\mu}{\rho} \cdot \frac{\partial^2 u}{\partial x^2}, \\
\frac{\partial^2 v}{\partial t^2} &= \frac{\mu}{\rho} \cdot \frac{\partial^2 v}{\partial x^2}, \\
\frac{\partial^2 w}{\partial t^2} &= \frac{\mu}{\rho} \cdot \frac{\partial^2 w}{\partial x^2}
\end{aligned} \tag{19}$$

The first equation in the relation (19) defines P-wave velocity V_P

$$V_P = \sqrt{\frac{k + 4\mu/3}{\rho}} = \sqrt{\frac{\lambda + 2\mu}{\rho}} \tag{20}$$

and the two following S-wave velocity, V_S, in the homogeneous media

$$V_S = \sqrt{\frac{\mu}{\rho}} \tag{21}$$

In the water, as well as other fluids, only ***P***-waves are spreading. The acoustic wave arrival causes pressure increase which forces movements of the water molecules toward each other. Intermolecular forces try to prevent such movements and move the molecules to their original locations. The final result of these opposite forces is seismic wave which is spreading only along the pressure increase direction only as ***P***-wave. In other words in fluids shear modulus μ is equal to 0, and the velocities of ***P*** and ***S*** waves are defined as follows

$$V_P = \sqrt{\frac{k}{\rho}} \qquad V_s = 0 \tag{22}$$

The results of the calculations ***P*** and ***S*** wave velocity, performed using the above equations, are shown on ***Fig.5***. Poisson's ratio s, rewritten in the form

$$\sigma = \frac{\left[(V_P/V_S)^2 - 0{,}5\right] - 1}{(V_P/V_S)^2 - 1} \tag{23}$$

is good indicator for lithology and fluid saturation. In the liquids it is equal to 0.5, and in the ideally hard rocks 0.25. Usually this ratio has values between 0.25 and 0.35, while in the unconsolidated sediments could even increase up to 0.40 and 0.45. A change of physical rock characteristics (lithology, porosity, fluid type and saturation, pressure) results in the change of ***P*** and ***S*** wave velocity and indirectly in the change of Poisson's ratio. If, for example, water or oil in the reservoir rock is replaced with very small amount of gas (even slightly bellow 5%), ***P*** wave velocity will drastically decrease, while the ***S*** wave velocity will show rather minor change.

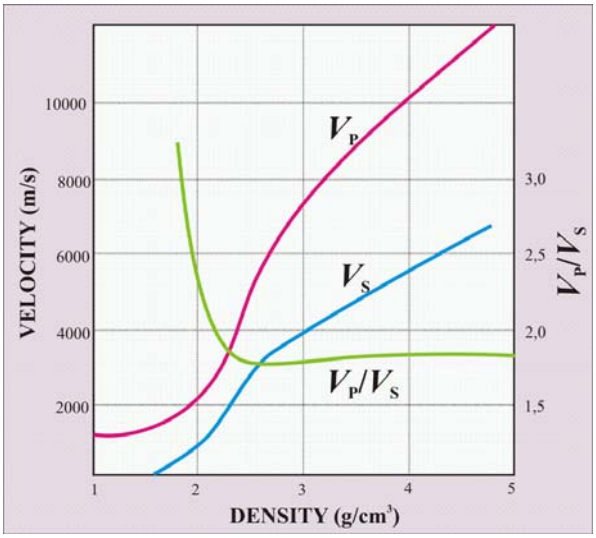

Fig.5: Relations between P wave velocity (VP), S wave velocity (VS), and their ratio (VP/VS) and density

Complex causal relations between elastic constants, density and seismic velocity according to the above equations and text obviously exist and could be successfully applied in lithology and fluid determinations on the basis of seismic data. Some of these relations are presented on ***Fig.6***. In the "soft" materials with small acoustic impedances (product velocity and density), like shale, a seismic wave arrival causes big particle movements and small pressure increase. For the "hard" materials with big acoustic impedances, like limestone, high pressure and small particle movements are characterizing seismic wave arrival.

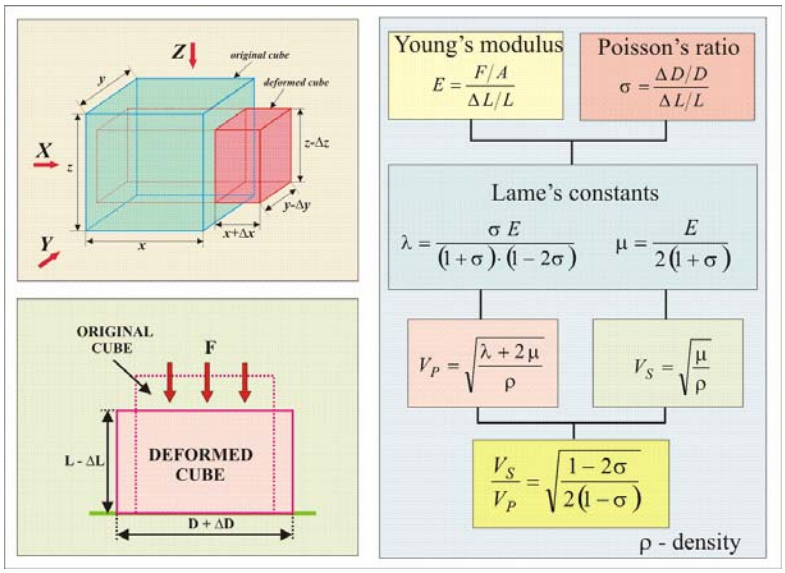

Fig.6: Relations between elastic constants and seismic velocities

Short summary of the effect of different rock properties on seismic ***P*** and ***S*** wave velocity and their ratio is presented on ***Fig.7*** (Tatham, 1991).

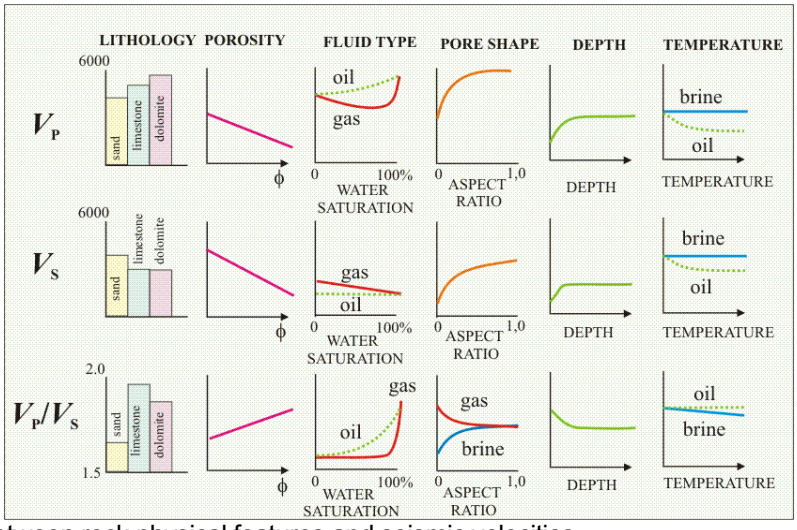

Fig.7: Relations between rock physical features and seismic velocities

Ranges of ***P*** and ***S*** waves velocities differ depending on lithology, in spite of certain overlapping, as shown on the first column on ***Fig.7***. The ***P*** wave velocity, V_P, is the highest in dolomite and the lowest in sand. Quite opposite situation is valid for ***S*** wave velocity, V_S, where the highest value is recorded in sands. As shown in the third row in the same column it has direct influence on V_P/V_S ratio. If porosity increases both velocities decrease. Faster decrease of shear wave velocity causes the increase of velocity ratio with porosity increase (the second column). Oil and gas saturations decrease, or water saturation increases, result in increase of ***P*** wave velocity, V_P, and decrease of ***S*** wave velocity, V_S, as shown in the third column. The velocity ratio, V_P/V_S, is increasing (the third row). It is important to notice that the same ratio in the gas saturated rock is constant until gas saturation became less than 5%. Increasing the aspect ratio, as shown in the fourth column, that is, more rounded pores; increase both ***P*** and ***S*** wave velocities. Increasing consolidation or depth of burial of rock increase both velocities and decrease their ratio. Temperature change causes both velocities changes only in oil saturated rocks, and very small change in velocity ratio.

AMPLITUDE VERSUS REFLECTION COEFFICIENT

Seismic waves on their way through the Earth underground change characteristics. When the seismic wave front strikes an interface, the wave is partially reflected in the first and partially transmitted into the second medium. Upon striking the interface at normal incidence, incident plane wave with unit amplitude produces reflection whose amplitude depends on acoustic impedance, i.e. on velocity-density product of each medium. Therefore the amplitude of the reflected wave is a function of the reflection coefficient, ***R***, defined by acoustic impedances, z_1 and z_2, products of densities, ρ_1 and ρ_2, and velocities, V_1 and V_2, of each medium, as follows

$$R = \frac{z_2 - z_1}{z_2 + z_1} = \frac{\rho_2 \cdot V_2 - \rho_1 \cdot V_1}{\rho_2 \cdot V_2 + \rho_1 \cdot V_1} \qquad (24)$$

The amplitude of the transmitted wave is defined by transmission coefficient which is equal to the relation

$$T = 1 - R = \frac{2 \cdot z_1}{z_2 + z_1} = \frac{2 \cdot \rho_1 \cdot V_1}{\rho_2 \cdot V_2 + \rho_1 \cdot V_1} \qquad (25)$$

As shown in the equation (25), amplitudes of reflected seismic waves are higher and have positive polarity, if the velocity is regularly increasing with depth. If the solution of the equation (25) is negative, as on the interfaces where bottom layer has lower acoustic impedance, the amplitude polarity change occurs. On the interfaces between seal rocks and reservoir gas saturated rocks very high reflected amplitudes are usually produced. The especially high reflected amplitudes, called bright spots, appear on the seismic sections recorded above gas reservoir rocks. One seismic section with this feature is shown on ***Fig.8***.

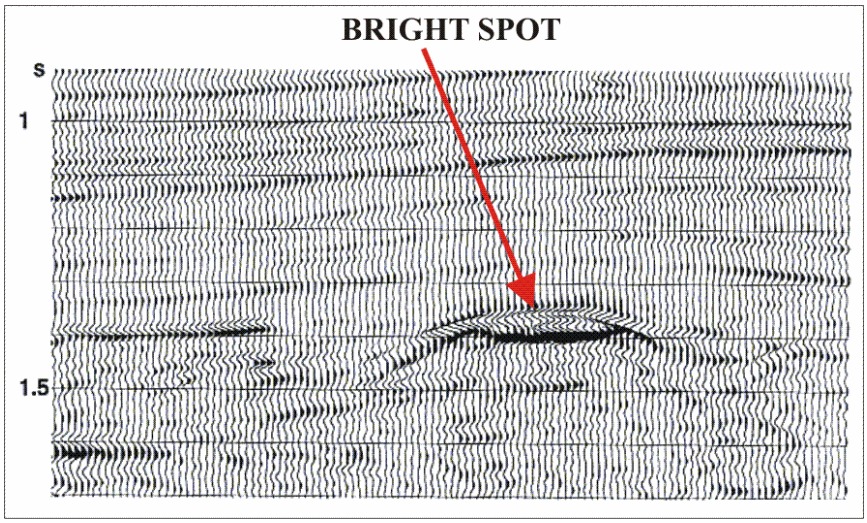

Fig.8: Bright spot effect

Every seismic wave arrival at the reflecting surface between two underground layers with an angle of incidence different from 90° results, as shown on ***Fig.9***, in the formation of four new seismic waves:

- Reflected ***P*** wave
- Reflected ***S*** wave
- Refracted ***P*** wave
- Refracted ***S*** wave

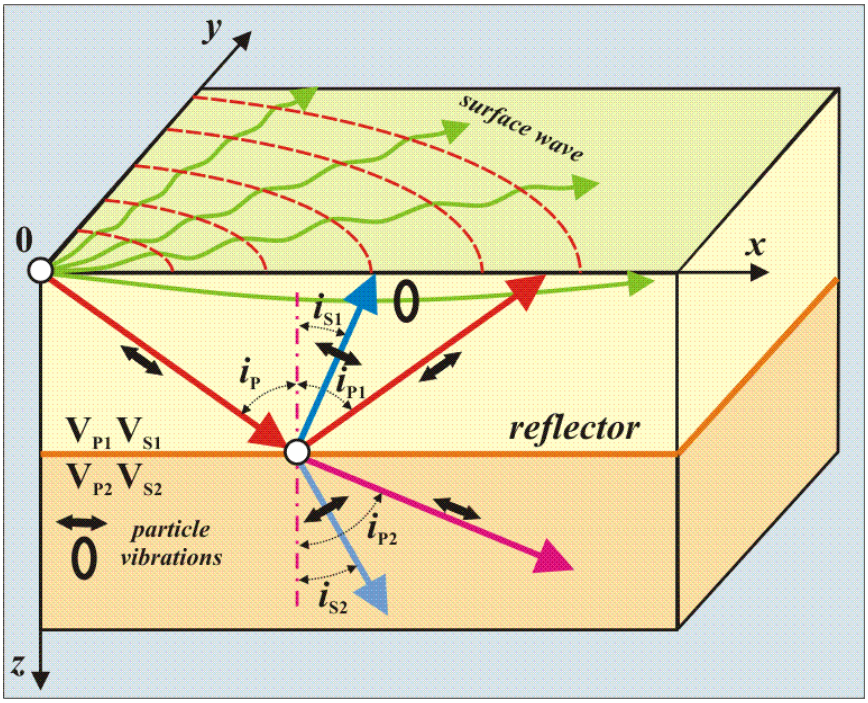

Fig.9: Seismic waves created on reflecting surface

According to Snell's low, ***P*** and ***S*** wave velocities and their angles of reflection and refraction exist following relations:

$$\frac{\sin i_p}{V_{p1}} = \frac{\sin i_{p2}}{V_{p2}} = \frac{\sin i_{s1}}{V_{s1}} = \frac{\sin i_{s2}}{V_{s2}} = p \qquad (26)$$

where

- V_{p1} – ***P*** wave velocity in the upper layer
- V_{p2} – ***P*** wave velocity in the lower layer
- V_{s1} – ***S*** wave velocity in the upper layer
- V_{s2} – ***S*** wave velocity in the lower layer
- i_P – angle of incidence
- i_{P1} – angle of reflection for ***P*** wave
- i_{S1} – angle of reflection for ***S*** wave
- i_{P2} – angle of refraction for ***P*** wave
- i_{S2} – angle of refraction for ***P*** wave
- p – seismic ray parameter

Seismic amplitudes, as well as their powers, are directly dependent on angles of incidence. On ***Fig.10*** normalized values of amplitude powers of reflected and transmitted ***P*** and ***S*** waves in two layer medium are shown. The ***P*** wave reflected amplitude is continually increasing as the angle of incidence increases, while the power of transmitted wave decreases and became zero at the angle of approximately 30^0. At the same angle reflected and transmitted ***S*** wave amplitudes quickly increased from zero to maximum value of 0.2 or 0.4. Further increase of the angle results in continuous decrease of both S amplitudes, and beyond the angle of 60^0 transmitted ***S*** wave ceased to exist.

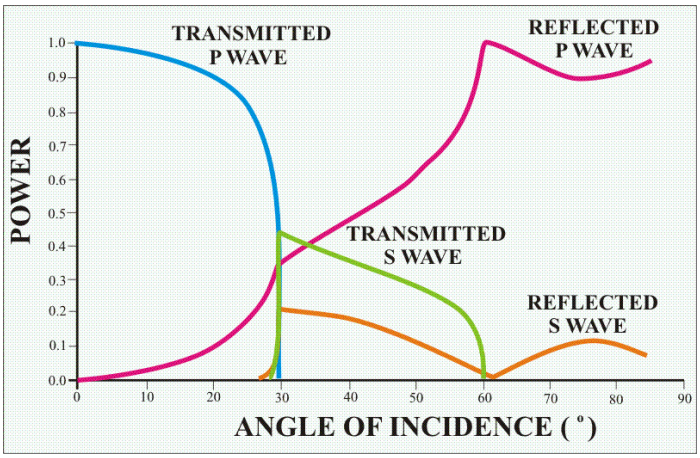

Fig.10: Amplitude vs. angle of incidence for reflected and refracted waves

By the application of Snell's low to the limiting conditions Knott-Zoepritz's equations are derived. They state that between reflection and transmission coefficients, angles of reflection and refraction, ***P*** and ***S*** wave velocities, and densities in two layers medium the following relations exist

$$(A_0 - A_1)\cdot \cos\alpha_p + B_1 \cdot \sin\alpha_s = A_2 \cdot \cos\beta_p + B_2 \cdot \sin\beta_s \qquad (27)$$

$$(A_0 + A_1)\cdot \sin\alpha_p + B_1 \cdot \cos\alpha_s = A_2 \cdot \sin\beta_p - B_2 \cdot \cos\beta_s \qquad (28)$$

$$(A_0 + A_1)\cdot \cos\alpha_s - B_1\left(\frac{V_{s1}}{V_{p1}}\right)\sin 2\beta_s = A_2\left(\frac{\rho_2 \cdot V_{p2}}{\rho_1 \cdot V_{p1}}\right)\sin 2\beta_s + B_2\left(\frac{\rho_2 \cdot V_{s2}}{\rho_1 \cdot V_{p1}}\right)\sin 2\beta_s \qquad (29)$$

$$\rho_1 V_{s1}^2\left[(A_0 - A_1)\sin 2\alpha_p - B_1\left(\frac{V_{p1}}{V_{s1}}\right)\cos 2\alpha_s\right] = \rho_2 V_{s2}^2\left[A_2\left(\frac{V_{p1}}{V_{p2}}\right)\sin 2\beta_p - B_2\left(\frac{V_{p1}}{V_{s2}}\right)\cos 2\beta_s\right] \qquad (30)$$

In the above equations the following symbols were used:

- A_0 – incident ***P*** wave amplitude
- A_1 – reflected ***P*** wave amplitude
- A_2 – refracted ***P*** wave amplitude
- B_1 – reflected ***S*** wave amplitude
- B_2 – refracted ***S*** wave amplitude
- V_{p1} – ***P*** wave velocity in the upper layer
- V_{p2} – ***P*** wave velocity in the bottom layer
- V_{s1} – ***S*** wave velocity in the upper layer
- V_{s2} – ***S*** wave velocity in the bottom layer
- ρ_1 – density of the upper layer
- ρ_2 – density of the bottom layer
- α_p – angle of reflection for ***P*** wave
- α_s – angle of reflection for ***S*** wave
- β_p – angle of refraction for ***P*** wave
- β_s – angle of refraction for ***S*** wave

Connections between reflection and transmission coefficients and angles of incident, or offsets, defined by Knott-Zoeppritz equations were extensively analyzed in order to establish usable correlation of seismic characteristics and rock physics. During years many simplified equations of these equations are derived and some of them proved to be

very useful in later developed AVO method. One of the most popular is the Shuey's (Shuey, 1985) approximation of reflection coefficient ***R(α)*** defined as follows

$$R(\alpha) \approx R_0 + \left[A_0 R_0 + \frac{\Delta\sigma}{(1-\sigma)^2} \right] \cdot \sin^2\alpha + \frac{\Delta V_P}{2 V_P} \left(tg^2\alpha - \sin^2\alpha \right) \qquad (31)$$

where are

$\tilde{R}(\alpha)$ – reflection coefficient at the normal incidence
σ – Poisson's ratio
α – angle of incidence
$\Delta V_P = V_{P2} - V_{P1}$
$V_P = (V_{P1} + V_{P2})/2$
$\rho = (\rho_1 + \rho_2)/2$
$\Delta_\rho = \rho_2 - \rho_1$

$$A_0 = B_0 - 2(1 + B_0)\left[\frac{1-2\sigma}{1-\sigma} \right]$$

$$B_0 = (\Delta V_P / V_P) / \left[\frac{\Delta V_P}{V_P} + \frac{\Delta\rho}{\rho} \right]$$

Upper and bottom layer are dented with indexes 1 and 2. Reflection coefficient at normal incidence is defined by the first part of the equation (31), while the second and the third part define reflection coefficients at the incident angle of 30^0 and 60^0. For the angle of incidence less than 30^0, the relation (31) could be approximately rewritten as

$$R(\alpha) \approx R_0 + B \sin^2\alpha \qquad (32)$$

where

$$B = A_0 R_0 + \Delta\sigma / (1-\sigma)^2 \qquad (33)$$

In the relations above ***R₀*** member is known as AVO intercept and the ***B*** member as AVO gradient. Accordingly, the dependence of the reflection coefficient ***R(α)*** on the angle of incidence for P waves is equal to the sum of the reflection coefficient at normal incidence and AVO gradient multiplied with the square of sinus function of the angle of incidence, ***α***.
In the relation (33) ***A₀*** is incident amplitude and ***σ*** Poisson's ratio.
Schematic synthetic presentation of seismic wave amplitudes, reflected from the top and the bottom of water and gas saturated sand layer, are shown on ***Fig.11.***

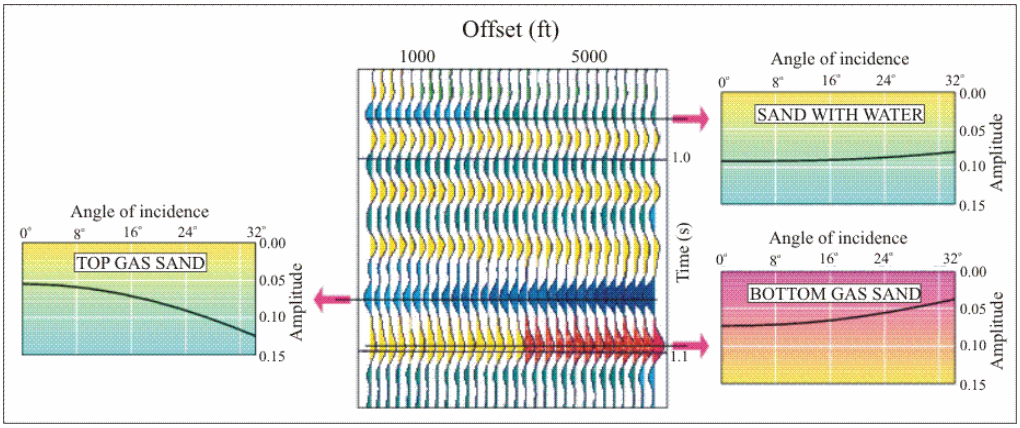

Fig.11: Amplitude change vs. offset and angle of incidence

The amplitude of the seismic wave reflected from the top of gas saturated sand layer, shown on the left side of the figure, increase if the angle of incidence increases. Its polarity became progressively more negative as the offset – dependent on the angle – increases, as shown on the section in the middle part. The reflected arrival from the gas sand bottom, shown at the right lower part of the figure, has the amplitude which became progressively more positive as the angle of incidence increases. Amplitudes reflected from the top of water saturated sand do not change if the angle of incidence or offset changes.

EXAMPLES FROM ADRIATIC SEA

North Adriatic area is located on the eastern foreland ramp of the Apennine Pleistocene foredeep basin as well as on the Dinarid fold and thrust belts, that involves platform (to the East) to basin (to the West) carbonates. Two main tectonic elements are present: the eastern slope of the Dinarid platform, striking NW-SE and NNW-SSE trending antiformal system related to the Dinarid compression phase. In the area several prospects in Pliocene turbidities and Miocene calcarenites associated with biogenic gas were pointed out. Stratigraphic traps in Lower Pliocene channels in the area also exist. The main reservoir rocks are loose shallow sands with porosities between 25 and 35%, filled with biogenic gas.
At the beginning of exploration campaign the main goal of the seismic data interpretation in the area was oriented to establish structural relations and locate the most prospective structural traps. Some discovered bright spot anomalies in the shallow part, like the one presented on ***Fig.12***, located above structural features were not particularly interesting at that time, mainly due to economical consideration (low gas price!).

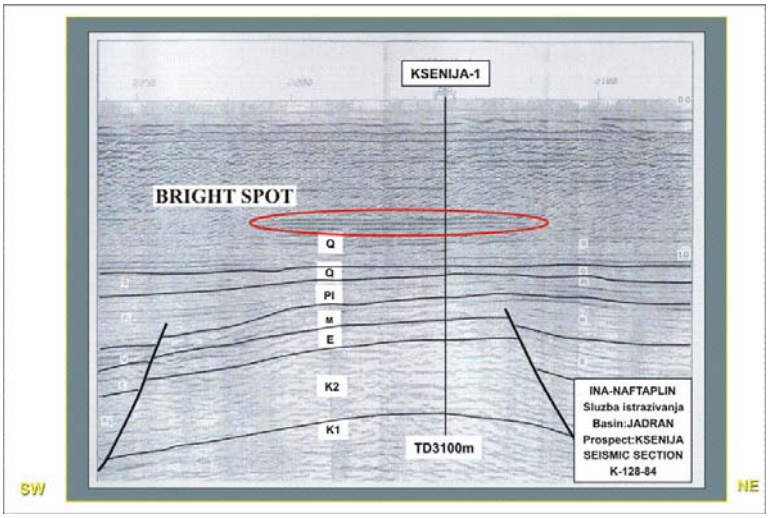

Fig.12: Typical bright spot anomaly in North Adriatic Sea

During structural interpretation it was noticed that some suspicious syncline forms exist on some possible very promising anticline structures. On ***Fig.13*** seismic line passing through such feature with well logs recorded in the well, are presented. At the first glance it seems that the syncline on the seismic section is not interesting at all. However, further analysis and already existing experience in seismic data interpretation in the area confirmed that the noticed push down effect is the cause of the shown false syncline at the top of structural gas trap.

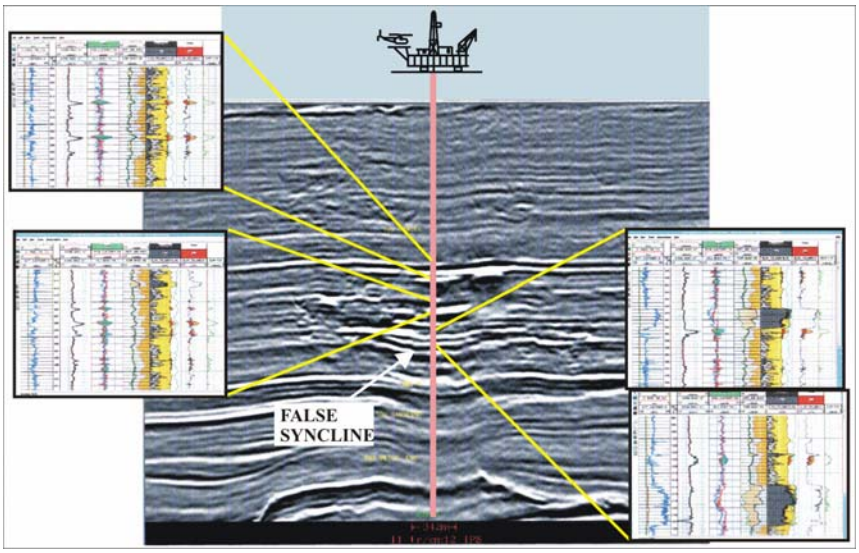

Fig.13: False syncline on 2D seismic section

Seismic time structure map of the surrounding area is shown on ***Fig.14***. Very strong anomalous amplitudes above these false synclines were caused with gas-filled rocks, with very low seismic velocities and the rocks above with normally higher velocities. The final result is the reflection with very strong amplitude and negative polarity ending with diffractions, as presented on the left hand side of the figure, well known as bright spot anomaly. Obviously such features on seismic profile and TWT map were caused by bright spot phenomena and not by poor data acquisition and processing, and definitely not by some locally developed small scale tectonic movements.

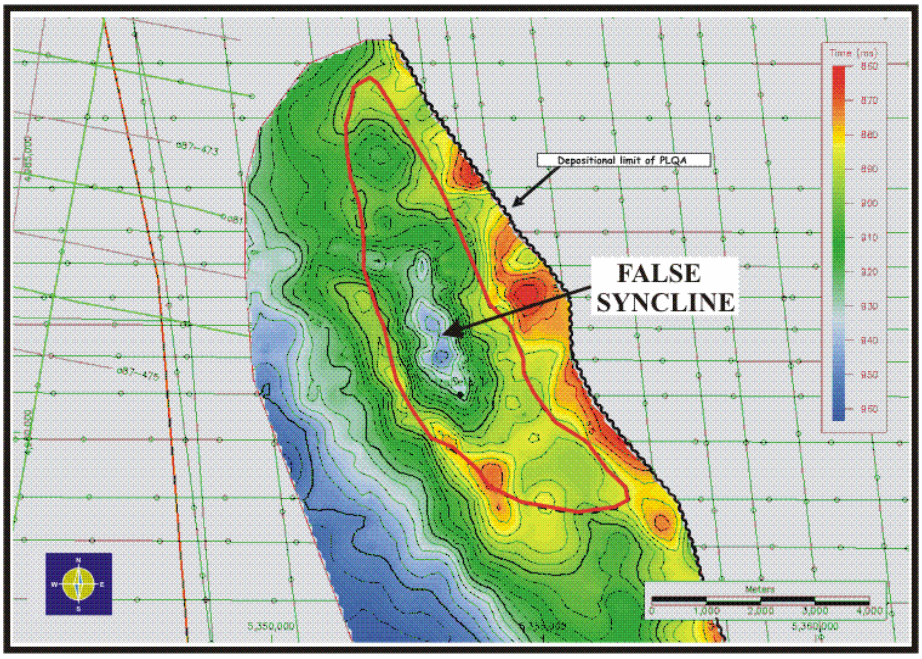

Fig.14: False syncline on seismic two-way-time structure map

On ***Fig.15*** two seismic lines with characteristic bright spot and pull down phenomena are presented. Very pronounced faulting on strong reflection bellow the areas with these effects shows that the bright spot, as well as the push down effects, were formed during

gas leaking through faults. In the marked areas gas accumulations were found above the deeper located faults.

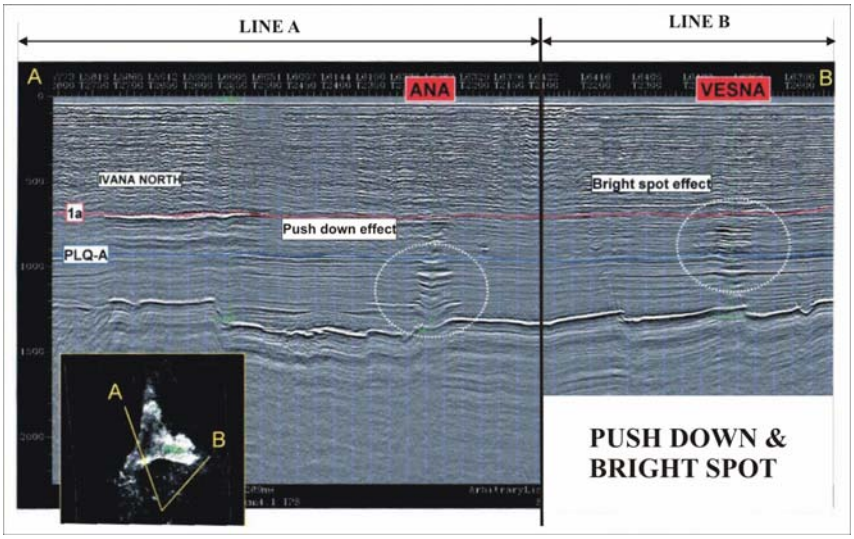

Fig.15: Bright spot and push down phenomena

Recently performed 3D seismic exploration acquisition campaign provided better quality data, enabled more sophisticated approach to bright spot interpretation using special AVO processing and increases the success ratio. The bright spot features with characteristic push down phenomena creating false syncline structure are clearly visible on the seismic section on ***Fig.16***. The located well was a success and proved that the strategy, based on the searching for bright spot effects, should be applied in the future.

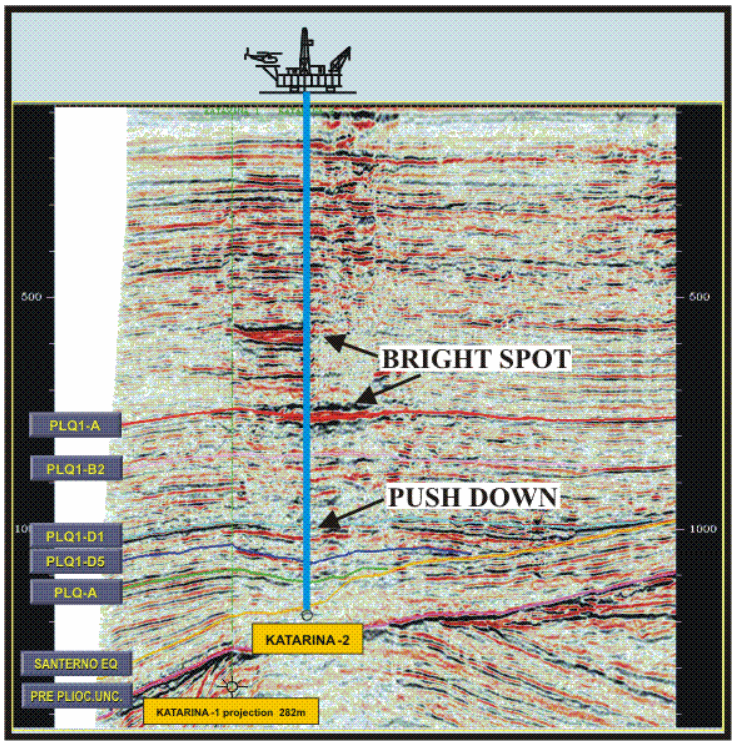

Fig.16: Bright spot effect above gas field

Seismic time structure map with amplitude strength map, shown in the area around the well on ***Fig.16***, is shown on ***Fig.17***. It shows good correlation between seismic time

structure map and amplitude strength and confirm that the “bright spot strategy” is the best exploration strategy for gas field exploration in north Adriatic Sea area.

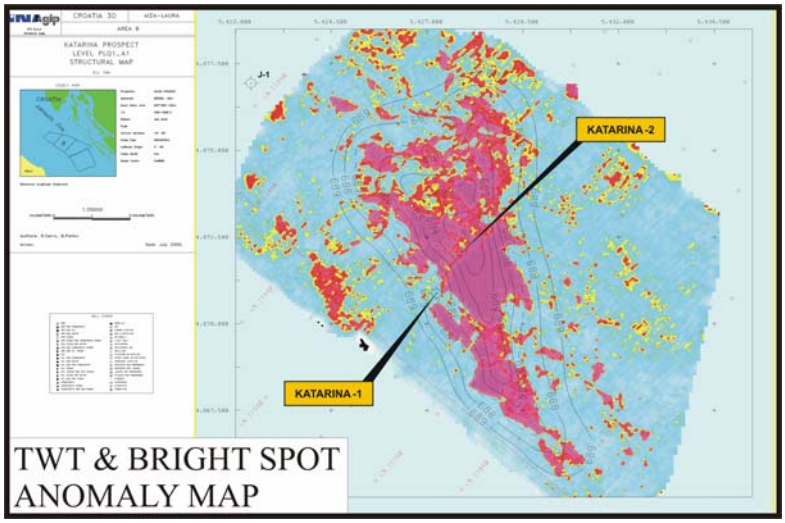

Fig.17: Seismic two-way-time structure map and amplitude strength map

According to the above very limited number of examples it is obvious that the search for bright spot phenomena, based on seismic reflection amplitude analysis, proved to be the most promising method in gas field exploration in North Adriatic area.

CONCLUSIONS

Relations between physical properties of rocks, theoretically established more than a century ago, proved to be very useful in seismic velocity and amplitude determination. Through the analysis of recorded seismic velocities and amplitudes using these relations it is possible to collect useful information concerning rock lithology and fluid saturation. These, however still more qualitative conclusions, proved to be practically very useful.
On the basis of these theoretical conclusions many gas fields were discovered in North Adriatic Sea, some of them already in exploitation. Previous interpretation of seismic data in order to locate possible structural traps was only partially successful. After some gas field discoveries in the area with strong bright spot phenomena, the new exploration strategy based on searching and analyzing such anomalies was successfully applied, resulting in more new producing gas fields.

Acknowledgement

The author would like to thank to the Exploration Department of INA d.d. Naftaplin Co. personnel for providing the material and valuable information necessary in the article preparation.

REFERENCES

1. Allen, J. L., Peddy, C. P., 1993: Amplitude variations with offset: Gulf Coast case studies: SEG Geophysical Development Series, 4

2. Anstey, N. A., 1990: The seismic pulse – Its generation and transmission: GP 202 Exploration Geophysiscs Series, IHRDC

3. Biancone, M., Mariani, M., 2000: Croatia offshore – Aziza Laura Block: Technical evaluation of the exploration potential, ENI AGIP/GEPE-ESPR

4. Bortfeld, R., 1961: Approximation to the reflection and transmission coefficients of plane longitudinal and transverse waves: Geophysics. Prosp., 9, 485-503

5. Castagna, J. P., Batzle, M. L., Kan, T. K., 1993: Rock physics – The link between rock properties and AVO response: u Catagna, J. P., Backus, M. M., eds., Offset-dependent reflectivity – Theory and practice of AVO anomalies, SEG Investigations in Geophysics no. 8, 135-171

6. Churlin, V. V., Sergeyev, L. A., 1963: Application of seismic surveying to recognition of productive part of gas-oil strata: Geolog. Nefti i Gaza, 7, p. 363

7. Forrest, M., 2000: Bright ideas still needed persistence: AAPG Explorer, 21, no. 5, 20-21

8. Gassman, F., 1951: Uber die elastizitat poroser medien: Vierteljahrsschr. Der Naturforsch. Gesellschaft Zurich, 96, 1-21

9. Geldart, L. P., Sheriff, R. E., 2004: Problems in exploration seismology and their solutions, SEG Geophysical References Series No. 14

10. Hilterman, F., 2001: Seismic amplitude interpretation: SEG, EAGE

11. Knott, C. G., 1899: Reflection and refraction of elastic waves with seismological applications: Phil. Mag., 48, 64-97

12. Koefoed, O., 1955: On the effect of Poisson's ratios of rock strata on the reflection coefficients of plane waves: Geophysics. Prosp., 3, 381-387

13. Mavko, G., Mukerji, T., Dvorkin, J., 1998: The rock physics handbook – Tools for seismic analysis in porous media: Cambridge Univ. Press.

14. Ostrander, W. J., 1982: Plane wave reflection coefficients for gas sands at nonnormal angles of incidence: Presented at the 52nd Ann. Internat. Mtg. Soc. Expl. Geophys., Expanded Abstracts, 216-218

15. Ostrander, W. J., 1984: Plane wave reflection coefficients for gas sands at nonnormal angles of incidence: Geophysics, 49, 1637-1648

16. Pan, P. P., de Bremaecker, J. C., 1970: Direct location of oil and gas by the seismic reflection method: Geophys. Prosp., 18, 712-727

17. Rosa, A. L. R., Frasier, C. W., 1976: Extraction of elastic parameters using seismic reflection amplitudes with offset variations: M.S. Thesis, Univ. Of Houston

18. Sengbush, R.L., 1983: Seismic exploration methods, IHDRC, Publishers, Boston, MA 02116, USA

19. Shuey, R. T., 1985: A simplification of the Zoeppritz equations: Geophysics, 50, 609-614

20. Wang, Z., Nur, A. M., 1992: Seismic and acoustic velocities in reservoir rocks – Theoretical and model studies, v. 2, SEG Geophysics Reprint Series, no. 10

21. Zoeppritz, K., 1919: Erdbebebwellen VIIIB, On the reflection and propagation of seismic waves: Gottinger Nachrichten, I, 66-84